International Journal of Frontiers in
Engineering and Technology Research
Journal homepage: https://frontiersrj.com/journals/ijfetr/
ISSN: 2783-0497 (Online)

(RESEARCH ARTICLE)

Check for updates

Influence of the marine engine load diagram characteristics on the ship propulsion system performance

Giovanni Benvenuto [1] and Ugo Campora [2,*]

[1] *DITEN - Department of Naval Architecture, Electrical, Electronic and Telecommunications Engineering, Polytechnic School, University of Genoa, Genoa, Italy.*
[2] *DIME - Department of Mechanical, Energy, Management and Transportation Engineering, Polytechnic School, University of Genoa, Genoa, Italy.*

International Journal of Frontiers in Engineering and Technology Research, 2022, 03(02), 056–067

Publication history: Received on 01 November 2022; revised on 15 December 2022; accepted on 17 December 2022

Article DOI: https://doi.org/10.53294/ijfetr.2022.3.2.0059

Abstract

In this study two four-stroke marine diesel engines, characterized by very similar nominal power and speed, but with very different trend of the power lint curve and specific fuel consumption contours in the engine load diagram, are compared by simulation, using each of them as an alternative to the other engine, for the motorization of a conventional (mechanical) propulsion plant for a small cruise ship. It is thus possible to determine and compare the efficiencies of the two engines and the vessel propulsion system overall performance for different ship speeds. The results of the comparisons are presented and discussed in the paper.

Keywords: Simulation; Marine engines; Diesel engines comparison; Ship propulsion plants

1. Introduction

The performance of a ship propulsion system depends on the characteristics of its components (mainly: propulsion engine, propeller, hull), whose choice must be framed in a correct propulsion plant design procedure defined according to the type and characteristics of the ship (i.e.: main dimensions, load capacity, design speed). In this procedure the hull and the propeller characteristics are preliminarily defined and optimized, in order to obtain the desired speed with minimum motion resistance and maximum propeller efficiency. Subsequently it takes place the choice of the most suitable engine for the defined propulsion plant. When choosing the engine, a very important parameter to consider is the engine Brake Specific Fuel Consumption (BSFC), to be minimized under engine Normal Continuous Rating (NCR) load conditions, corresponding to the vessel design browsing speed, with an appropriate value of the engine margin.

This procedure for optimizing the propulsion system, in addition to reducing fuel consumption during navigation, is also aimed, last but not least, at making the system itself in compliance with the increasingly restrictive international limits for the protection of the environment, in particular with reference to carbon dioxide emissions, as required by the regulations promoted by the International Maritime Organization (IMO) [1-4] regarding the EEDI (Energy Efficiency Design Index) and/or EEOI (Energy Efficiency Operation Index) indicators.

However, in some types of vessels, as cruise ships and ferries, the speed of navigation can vary significantly depending on the distance between the ports of departure and arrival and the relative navigation time, the latter conditioned by the travel schedule. In these ships the propulsion engine often works in conditions very different from those corresponding to the NCR, so the efficiency of the engine depends on the power limit-speed curve and specific fuel consumption contours trend and on the values assumed by this last parameter in the engine operating diagram.

* Corresponding author: Ugo Campora

More generally, the optimization of a naval propulsion system depends on how the problem of matching the ship's and the propeller characteristics with those of the engine, in terms of power-rpm of its load diagram, is solved. For ships characterized by predominantly constant speed, the matching problem is solved by adopting appropriate values for the Sea Margin, the Engine Margin and the reduction ratio of the reduction gear, if present, in order to optimize the efficiency of the engine for its prevalent operating condition. Otherwise, for ships with frequent speed variations, it is necessary to optimize the efficiency of the engine in a wide range of variation in power and rpm within the engine load diagram. In some cases it may also be convenient to adopt variable pitch propellers, as shown in some of the author papers, both for a conventional propulsion system, of a mechanical type [5,6], and for an unconventional propulsion system of the CODLAG type [7].

In this article, starting from a simulation model of the propulsion system [8], developed for a small cruise ship using two identical 4-stroke diesel engines, the engines originally adopted are replaced, by simulation, with two engines of another manufacturer, both characterized by powers and speeds very similar to those of the original engines. The new engines belong to the series called 'Bergen', manufactured by Rolls-Royce [9] The Bergen diesel engines are subdivided into two subseries, one characterized by 900 rpm of maximum speed and the other by 1000 rpm; the engines are characterized by very similar Maximum Continuous Rating (MCR), but they differ significantly in the power limit curve and in the BSFC contours trend in the engine load diagram.

The author intention is to carry out an investigation on the effect of the marine engines load diagram power limit curve and specific fuel consumption contours trend has on the performance of a mechanical ship propulsion system. In the article two diesel engines are compared between them, but the same comparison can be made between engines fuelled with an unconventional fuel, such as natural gas, or with possible future alternative marine fuels, such as: hydrogen, methanol and ammonia.

In the paper both versions of the Bergen engine are used as alternative to the original engine in the propulsion system of the small passenger ship. The performance of the two engine versions and the overall efficiencies of the respective propulsion systems are analyzed and compared, for different ship speeds. The results of the comparisons are presented and discussed in the paper.

2. Diesel engines and ship propulsion plant

The vessel considered for this research is the small cruise ship Spirit of Oceanus of the Cruise West shipowning company. Fig. 1 shows the propulsion plant configuration, composed by two independent axis lines; in each shaft a four stroke diesel engine (MAIN-DE in figure) drives, through a reduction Gear (G), a Controllable Pitch Propeller (CPP). During navigation the ship hotel electric load is satisfied by two Shaft Electric Generator (SEG), directly mounted in each engine shaft as shows in Fig. 1.

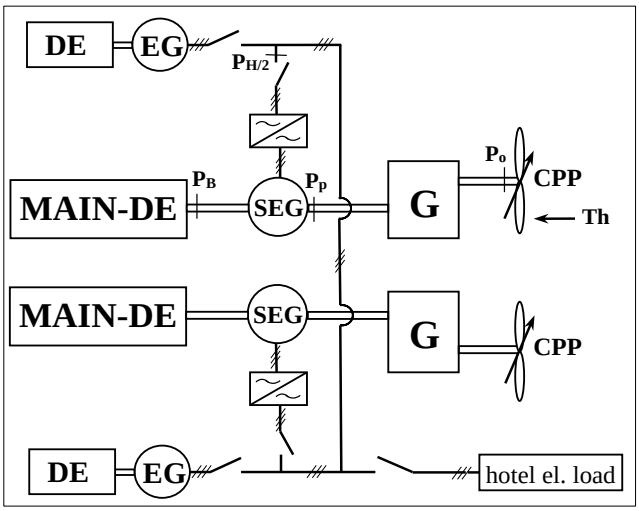

Figure 1 Ship propulsion plant scheme with shaft electric generators

The two diesel electric generators (DE-EG blocks in Fig. 1) are used only with the ship on port.

The main data on the ship and the original propulsion plant are reported in Tab. 1.

Table 1 Main ship data

Overall length	80.7 m
Breadth	15.3 m
Draught	3.9 m
Displacement	3000 t
Maximum speed (design draught)	18.5 kn
Original propulsion diesel engines	2x2289 kW
Shaft electric generators	2x800 kWe
Diesel generators	2x1050 kWe
Summer hotel electric power	984.7 kW
Winter hotel electric power	727.8 kW
Passenger	120
Crew	72

Tab. 2 reports the main characteristics of the original adopted diesel engines (General Electric GE12V228) and of the new engines compared in this paper: Rolls-Royce Bergen C25:33L8P-900/1000 rpm of maximum speed (N_{max}) [9].

Table 2 Engines main data and performance parameters at MCR conditions

Engines parameters	**GE 12V 228**	**RR C25:33L8P 900 rpm N_{max}**	**RR C25:33L8P 1000 rpm N_{max}**
Cylinder numbers	12	8	8
Bore	228.6 mm	250.0 mm	250.0 mm
Stroke	266.7 mm	330.0 mm	330.0 mm
Brake power	2289 kW	2560 kW	2665 kW
B.m.e.p.	19.9 bar	26.4 bar	24.7 bar
Maximum speed	1050 rpm	900 rpm	1000 rpm
Norm. MCR BSFC	-	0.875	0.890

In Tab. 2 B.m.e.p. is the brake mean effective pressure. In the same table the BSFC of the Rolls-Royce Bergen engines is normalized by dividing it by that of the GE12V228 engine, with reference to the MCR load conditions.

Fig. 2 shows the power limit curves and the normalized BSFC contours, in the power-speed operating diagram, of the considered Bergen C25:33L8P engines, the first characterized by 900 rpm N_{max} (Fig. 2a) and the second by 1000 rpm N_{max} (Fig. 2b) [9].

From the figure it can be observed the very different trend of the BSFC contours and of the power limit curves that characterize the two engines versions (unfortunately similar data are not available for the GE12V228 engine). The BSFC contours of the 900 rpm N_{max} engine (Fig. 2a) are characterized by a shape similar to that of most marine engines of the same category [5,6,10,11,12]. The BSFC contours of the 1000 rpm N_{max} engine are instead characterized by a particular trend, that the authors have not found in any other similar engine with a single turbocharger. As shown in Fig. 2b, the BSFC contours characterized by a lower specific fuel consumption, have a tendency that brings them closer to each other near the power limit curve, when the engine speed decreases. Consequently this engine is characterized by high efficiency even at reduced rpm when it works just below the power limit curve. According to manufacturer's indications,

the remarkable difference in the BSFC contours of these two engines is due only to the different tuning, while the trend of the power limit curves is determined by engine toque or turbocharger compressor surge limits.

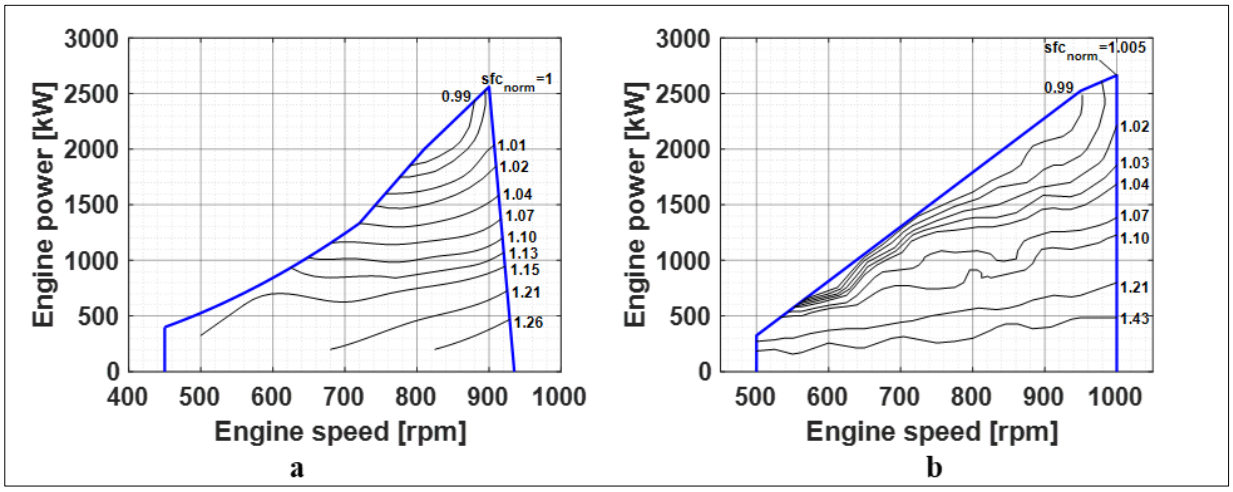

Figure 2 Power limit curves and normalized specific fuel consumption contours of the Bergen engines on the power-speed operating diagram

3. Propulsion plant simulator

In order to determine the running data of the main components of the propulsion plant (PP) for the considered cruise ship, an already presented simulator [8] was used, developed in Matlab©-Simulink© language. Each simulator block shown in Fig. 3 reproduces the corresponding component of the propulsion system considered in Fig. 1. Fig. 3 shows only the simulator blocks relating to the propulsion plant starboard part, being the portside of the same specular to the first.

It is important to note that in this application the PP simulator is used only to obtain, for selected ship speeds, the propeller torque (*Q_P*) and speed (*N_P*, in rpm), and therefore the power absorbed by the propeller (P_p, see upper shaft line in Fig. 1). For this reasons in this paper the engine simulation model (applied to GE12V228 engine) is described very briefly.

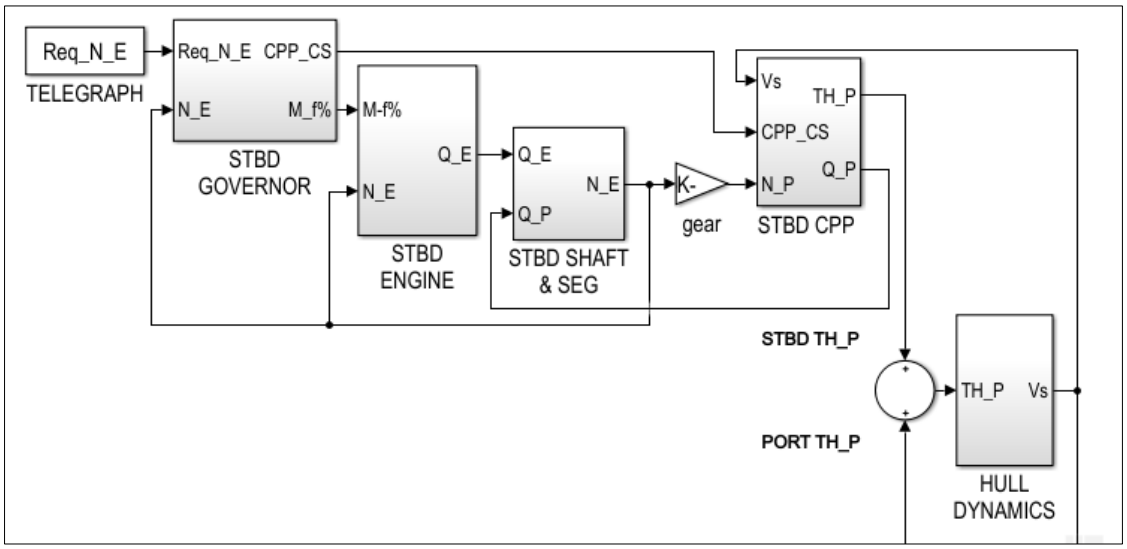

Figure 3 Simulink scheme of the ship's starboard propulsion plant

The Simulink blocks of Fig. 3 are: the telegraph: 'telegraph', the engine and CPP controller: 'stbd governor', the diesel engine: 'stbd engine', the shaft line and SEG: 'stbd shaft and seg', the gear: 'gear', the controllable pitch propeller: 'stbd

cpp', the ship dynamics: 'hull dynamics'. Each simulator block provides the performance of the propulsion plant corresponding component, by means of functions, tables, differential and algebraic equations.

A brief description of the simulator modules is provided below, while a more detailed treatment can be found in [5,6,8].

3.1. HULL DYNAMICS module

In the 'hull dynamics' block the ship's longitudinal speed (*Vs*) is determined by the dynamic equation:

$$\frac{dVs}{dt} = \frac{TH_p - TH_s}{m_s + m_{ad}} \quad \text{..... (1)}$$

where: t is the time, m_s is the ship mass and m_{ad} the added mass. The hull resistance is modelled by a 1-D table as a function of the ship speed: the thrust required by the hull (TH_s) is determine by the equation: $TH_s = R/(1\text{-}t)$, where R is the towing tank resistance and t is the thrust deduction factor. The propeller thrust (TH_p in eq. (1)) is determined in the below described CPP module.

3.2. STBD CPP module

For the adopted controllable pitch propeller, the open water characteristics consist of a set of K_T and K_Q curves, functions of the advance coefficient J and of the pitch/diameter ratio (P/D), according to the model reported in [13] The inputs of the module are the ship's speed V_S (coming from the 'hull dynamics' block), the P/D value (*CPP_CS* from the 'stbd governor' module) and the propeller shaft speed (*N_P* from the 'gear' block).

3.3. STBD SHAFT & SEG module

This simulator block determines the engine shaft speed (*N_E*) by means of the shaft dynamic equation:

$$\frac{dN_E}{dt} = \frac{1}{2\pi J'}\left(Q_E - Q_P - Q_{SEG}\right) \quad \text{..... (2)}$$

where: J' is the inertia of the rotating masses, Q_E, Q_P and Q_{SEG} are the engine, the propeller and the SEG torque respectively. The engine and propeller torques (Q_E and Q_P) are the module inputs. The SEG torque depends on the electric power values (in summer or winter, reported in Tab. 1) and on the engine shaft speed (*N_E*).

3.4. STBD ENGINE module

The Simulink 'stbd engine' module is in turn divided into sub-models, each of which reproduces the operation of each of the engine components, which are: cylinder, intercooler and air receiver, exhaust gas receiver, turbocharger compressor and turbine. Each engine component is modelled by algebraic, differential equations and tables. A zero dimensional filling and emptying approach is employed in the diesel engine simulator. As reported in more detail in [5,8], for the cylinder calculation the crank angle (θ) is the independent variable.

The cylinder inlet and outlet mass through the respective valves are determined with the classic gas dynamic equations for compressible gas through a duct restriction [14]. The convective gas-cylinder wall heat transfer is determined as reported in [15]. [The delay angle is evaluated as reported in [16]. During the combustion phase, the fuel fraction burned is determined by the Wiebe equation [17]. During the compression, combustion and expansion phases the pressure inside the cylinder is calculated by applying the dynamic energy balance equation [8].

The air and exhaust gas receiver and the turbocharger are modelled as reported in [5]; in the same paper the procedure for the calculation of the engine brake torque (Q_E in Fig. 3) is described.

3.5. STBD GOVERNOR module

The governor of the propulsion plant, of the PID (proportional integral derivative) type, is modeled in the 'stbd governor' block of Fig. 3. The governor inputs are: the required engine speed (*Req_N_E* from the 'telegraph' block of Fig. 3) and the actual one (*N_E*). The governor controls the engine fuel flow percentage (*M_f*%), in order to maintain the required engine speed (*Req_N_E*), and the propeller P/D value (through the *CPP_CS* block output variable). The *N_E* - P/D combined law depends on the adopted engine type, as shown further on.

4. Engines working conditions

As mentioned above, the ship propulsion plant simulator is used to obtain, for the selected ship speed (13, 14, 15, 16, 17, and 18 knots are considered), the propeller torque (*Q_P*) and speed (*N_P*), from the 'stbd engine' and 'stbd shaft and seg' modules respectively (see Fig. 3), and therefore the power absorbed by the propeller (P_o, see upper shaft line in Fig. 1) by equation:

$$P_o = Q\_P\ 2\ \pi\ N\_P/60 \quad \text{..... (3)}$$

The propulsion power (P_p), upstream of the SEG (Fig. 1), is determined with the equation:

$$P_p = \frac{P_o}{\eta_R \eta_G \eta_S} \quad \text{..... (4)}$$

where: η_G and η_S are the gear and the shaft efficiencies respectively, and η_R is the propeller's relative rotary efficiency. In the present application the values of these efficiencies are assumed as follows: η_G = 0.98, η_S = 0.98, η_R = 0.99.

In order to calculate the engine brake power (P_E in Fig. 1), in addition to the power to drive the propeller, it is necessary to consider the power supplied to the shaft electric generator, by equation:

$$P_E = P_p + \frac{P_H/2}{\eta_{AC/AC}\eta_{SEG}} \quad \text{..... (5)}$$

with: P_H the ship hotel electric power (whose values in summer and winter are shown in Tab. 1), $\eta_{AC/AC}$ the electric frequency converter efficiency and η_{SEG} the shaft electric generator efficiency. In this application the values of these efficiencies are: $\eta_{AC/AC}$ = 0.97; η_{SEG} = 0.96.

As mentioned above, the two Bergen engines selected to replace the original engine of the considered cruise ship, are characterized by a different maximum rotational speed, the first 900 rpm N_{max} and the second 1000 rpm N_{max}.

Considering a reference maximum ship speed of 18 knots, and that this speed is obtained with the Bergen C25:33L8P engines working at their respective maximum speeds, a gear speed ratio (G_R), defined as:

$$G_R = \frac{N_E}{N\_P} \quad \text{.....(6)}$$

can be calculated for the two engines, resulting clearly different from each other due to the different maximum rpm of the engines (900 rpm N_{max} and 1000 rpm N_{max}). The G_R value obtained for a specific Bergen engine is evidently kept constant as the speed of the ship changes.

By applying the calculation procedure described above, it was possible to determine, for a maximum ship speed of 18 knots, the working conditions of each of the considered Bergen engines, as shown in the load diagrams of Fig. 4. In the figure the black marker indicates the propulsion power (P_p, determined by eq. (4)), while the magenta and yellow markers represent the overall power of the engine (P_E, calculated with eq. (5)), in summer (magenta) and winter (yellow) navigation.

Again with reference to a maximum ship speed of 18 knots, the propeller torque (*Q_P*) and speed (*N_P*) determined by the simulator refer to a propeller pitch/diameter ratio (*P/D*) of 1.05.

For the sake of good engine management, it was decided that the minimum value of the engine margin (difference between the limit power and the maximum power supplied by the engine, at the same speed) should not be less than 10%. Obviously the maximum power delivered by the engine is that relating to summer navigation (magenta markers in Fig. 4).

The condition on the engine margin mentioned above, with a propeller P/D ratio of 1.05, is respected in both Bergen engines only for ship speeds of 18 and 17 knots.

The 900 rpm N_{max} Bergen engine does not comply with the engine margin condition for ship speeds below 17 knots. As can be seen from Fig. 4a, this is due to the power limit curve trend, which shows a tendency to curve downwards at the reduction of the engine speed, compared to that of the 1000 rpm N_{max} Bergen engine (Fig. 4b).

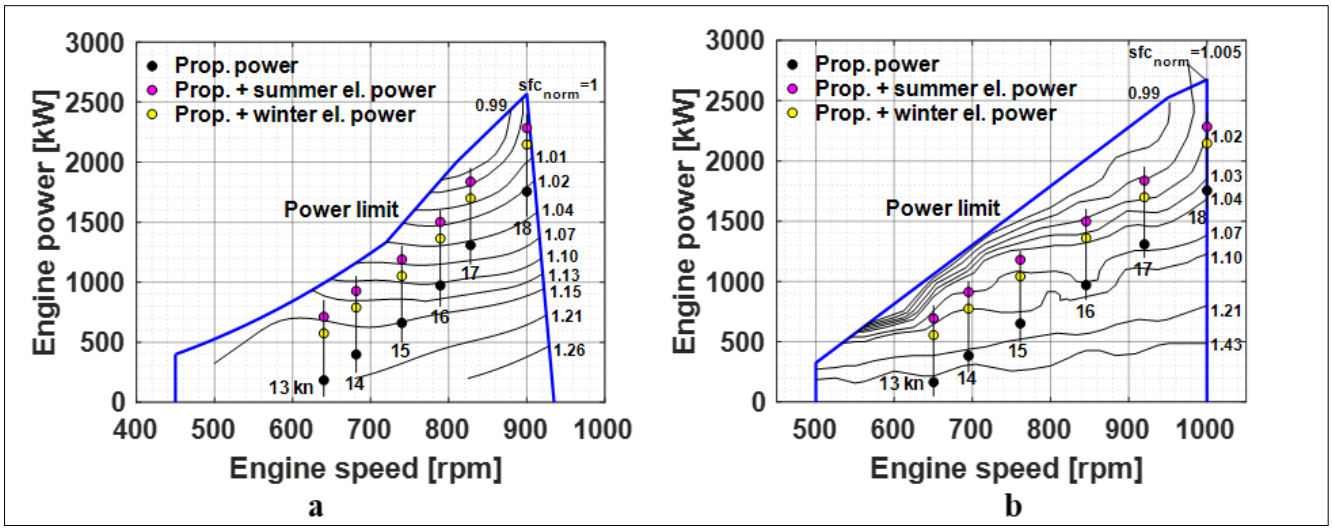

Figure 4 Working conditions, in the load diagram (power-rpm), of the considered Bergen engines, with N_{max} = 900 rpm (a) and N_{max} = 1000 rpm (b), as function of the ship speed

To comply with the chosen margin engine, as the ship speed decreases, the propeller *P/D* ratio has to be progressively reduced, as shown in Fig. 5. In this figure it can be seen that the CPP *P/D* ratio reduction starts at a ship speed of 16 knots, in the case of 900 rpm N_{max} Bergen engine, while the propeller *P/D* ratio reduction starts at a ship speed of 14 knots in the case of 1000 rpm N_{max} Bergen engine.

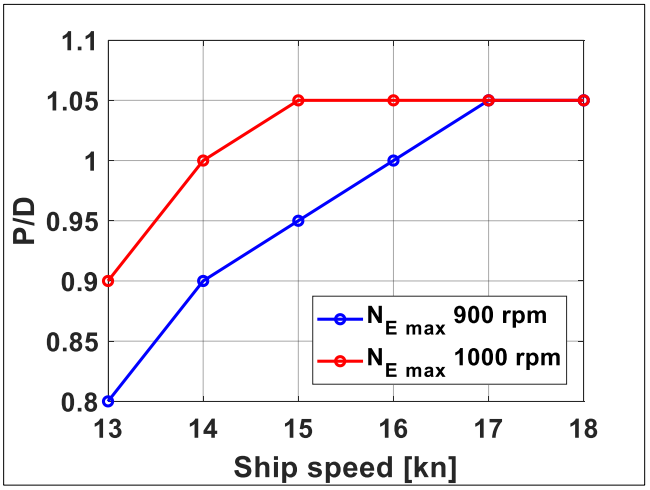

Figure 5 P / D ratio variation laws for the CPP propeller versus the ship speed

With a lower propeller *P/D* ratio, in order to obtain the required thrust for the desired ship speed, it is necessary to increase the propeller shaft speed, and therefore the engine one, thus bringing the relative operating point to a number of revolutions for which the value of the engine power limit is higher, as shown in Fig. 4.

It is important to observe that reducing the *P/D* ratio of the propeller implies less propeller efficiency [13], with the same propulsion thrust, and thus increases the engine required power.

5. Bergen engines comparison

This paragraph presents the main results of the comparison between the two Bergen engines selected for the propulsion system of the considered cruise ship. The comparison is made considering the engine with 900 rpm N_{max} as the reference engine, this being characterized by a more 'typical' BSFC contours trend in the power-speed operating diagram (see Fig. 2a).

Fig. 7 shows the brake power percentage difference between the 1000 rpm N_{max} engine and the 900 rpm N_{max} one, as function of the ship's speed, in case of summer and winter navigation. The brake power difference between the two engines is determined by the generic equation:

$$\Delta x/x\% = \frac{x_{1000\,\text{rpm}\,N\,\text{max}} - x_{900\,\text{rpm}\,N\,\text{max}}}{x_{900\,\text{rpm}\,N\,\text{max}}} 100\ [\%] \quad \text{..... (8)}$$

with: x the generic variable, $x_{900\,\text{rpm}\,N\,\text{max}}$ and $x_{1000\,\text{rpm}\,N\,\text{max}}$ are the generic variable (x) referred to 900 rpm N_{max} and 1000 rpm N_{max} Bergen engines respectively. The equation (8) is used to generate the data reported in the Figs. 7 and 9.

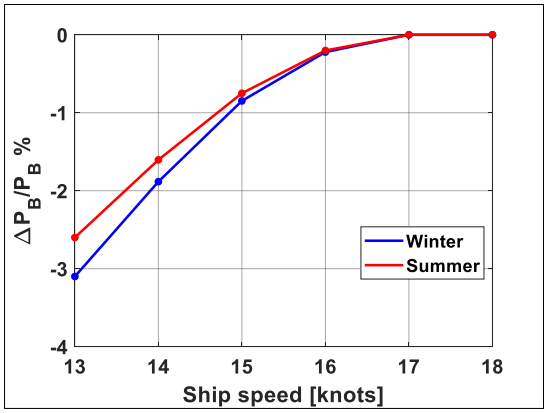

Figure 7 Percentage difference of the brake power between the 1000 rpm and the 900 rpm N_{max} engines, as function of the ship's speed, in case of summer and winter conditions

Fig. 7 shows that the 900 rpm N_{max} Bergen engine develops a greater brake power, compared to the 1000 rpm N_{max} engine, under a ship speed of 16 knot.

This difference, which increases as the ship speed decreases and in winter navigation, is due to the already mentioned request for a lower propeller P/D ratio by the 900 rpm N_{max} Bergen engine compared to the 1000 rpm N_{max} one, as shown in Fig. 5. This implies a lower propeller efficiency (at parity of thrust), which translates into a greater demand for brake power by the engine (see eqs. from (3) to (5)). The above considerations on the brake powers of the two engines confirm the results presented in Fig. 4 on the working conditions of the same engines in the respective load diagrams as a function of the ship's speed in both summer and winter conditions.

Between the two engines in comparison a clearly significant aspect regards the thermodynamic efficiency, given by the equation:

$$\eta_E = \frac{P_B}{M_f H_f} \quad \text{..... (9)}$$

where: P_B is the engine brake power, M_f and H_f the fuel mass flow rate and its lower heating value respectively.

The engines efficiency values, for varying ship speeds, in winter and summer navigation, are shown in Fig. 8a. The figure shows the slightly higher efficiency of the 900 rpm N_{max} engine, compared to the 1000 rpm N_{max} one, for a ship speed of 18 and 17 knots, while the efficiencies are substantially the same for a ship speed of 16 knots.

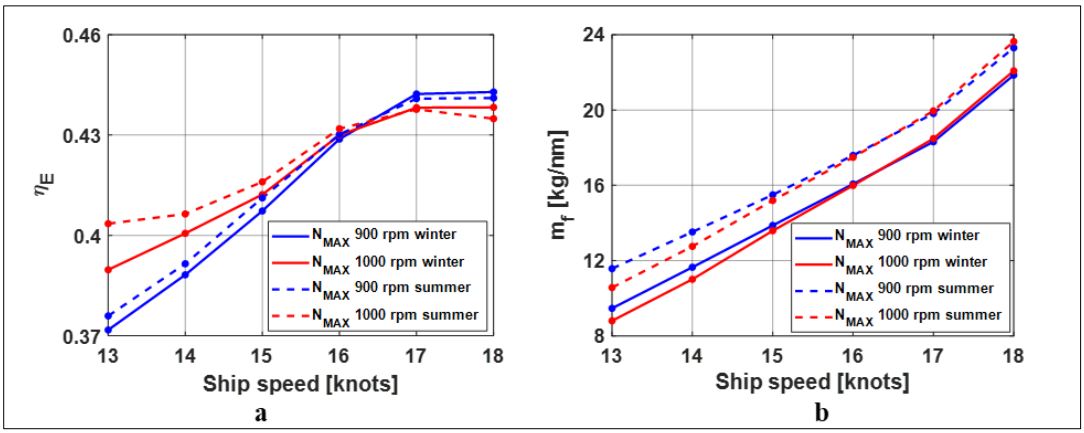

Figure 8 900 and 1000 rpm N_{max} engines overall efficiency (a) and fuel consumption per nautical mile (b) for different ship's speeds in winter and summer conditions

On the contrary, below 16 knots of ship speed, the efficiency of the 1000 rpm N_{max} engine becomes more and more greater, as the ship speed decreases, compared to that of the 900 rpm N_{max} engine. This behaviour is explained by comparing the different operating conditions of the two engines, in the respective load diagrams, for the different ship speeds considered, as shown in Fig. 4 (yellow markers for winter conditions and magenta markers for summer ones).

Indeed, for ship's speeds of 18 and 17 knots, the 900 rpm N_{max} engine (Fig. 4a) operates in a zone characterized by less values of the specific fuel consumption, compared to the 1000 rpm N_{max} engine (see Fig. 4b).

Instead, for ship's speeds less than 16 knots, it is the 1000 rpm N_{max} engine to operate in an area characterized by lower values of the specific fuel consumption, compared to the 900 rpm N_{max} one (see Figs. 4a and 4b). The growing efficiency difference between the two engines, which is observed in Fig. 8a as the ship speed decreases from 15 knots, is due to the significantly different trend of the specific fuel consumption contours of the two engines (Figs. 4a and 4b), where the engines operate at the aforementioned ship speeds.

Fig. 8b shows the mass of fuel needed by the ship to travel one nautical mile in calm sea conditions. Obviously, given the greater electrical power required in summer navigation (see Fig. 4), the consumed fuel mass is greater in the summer navigation for both the considered engines. As regards the comparison between the engines, Fig. 8b shows that the fuel consumption per nautical mile is very similar for the two engines, for ship's speeds between 16 and 18 knots, while for lower speeds (under 16 knots) the 900 rpm N_{max} engine consumption is getting higher and higher, compared to the 1000 rpm N_{max} one.

In order to offer a more detailed analysis of the comparisons shown in Fig. 8, Fig. 9 shows the same data, but processed, by means of Eq. (8), in the form of percentage differences, relating to winter and summer navigation, always for different ship speeds.

Fig. 9a shows the percentage differences between the two Bergen engines regarding engine efficiency for different ship's speeds. From the figure it can be observed that for ship speeds between 17 and 18 knots the 900 rpm N_{max} engine is characterized by an efficiency higher than that of the 1000 rpm N_{max} one by about 1%. This advantage is reduced to zero when the ship's speed decreases from 17 to about 16.3 knots. These considerations are generally valid for both between 17 and 18 knots the 900 rpm N_{max} engine is characterized by an efficiency higher than that of the 1000 rpm N_{max} one by about 1%. This advantage is reduced to zero when the ship's speed decreases from 17 to about 16.3 knots. These considerations are generally valid for both winter and summer navigation. Starting from about 16 knots, as the ship's speed decreases, the efficiency of the 1000 rpm N_{max} engine becomes progressively greater than that of the 900 rpm N_{max} one, until reaching an advantage of about 5% at a speed of 13 knots in winter navigation, and greater than 7%, at the same speed, in the summer one.

The fuel consumption per nautical mile percentage comparison, for different ship speeds, reported in Fig. 9b, shows that, coherently with the data shown in Fig. 9a, the navigation with the 900 rpm N_{max} engine leads to a lower fuel consumption for nautical mile of about 1%, compared to 1000 rpm N_{max} engine, for ship speeds between 17 and 18 knots. This advantage gradually decreases to zero between 17 and about 16.4 knots of ship speed. Below this speed value (16.4 knots) and further ship speed decreasing, the 1000 rpm N_{max} engine allows a constantly increasing fuel

savings, compared to the 900 rpm N_{max} one, up to about 7%, in winter navigation at ship speed of 13 knots, and above 8.5% in summer navigation at the same speed. Fig. 9b also shows that the percentage differences in fuel consumption per nautical mile remain substantially the same in both winter and summer navigation cases, for the different speeds of the ship, with the sole exception of the speed of 13 knots.

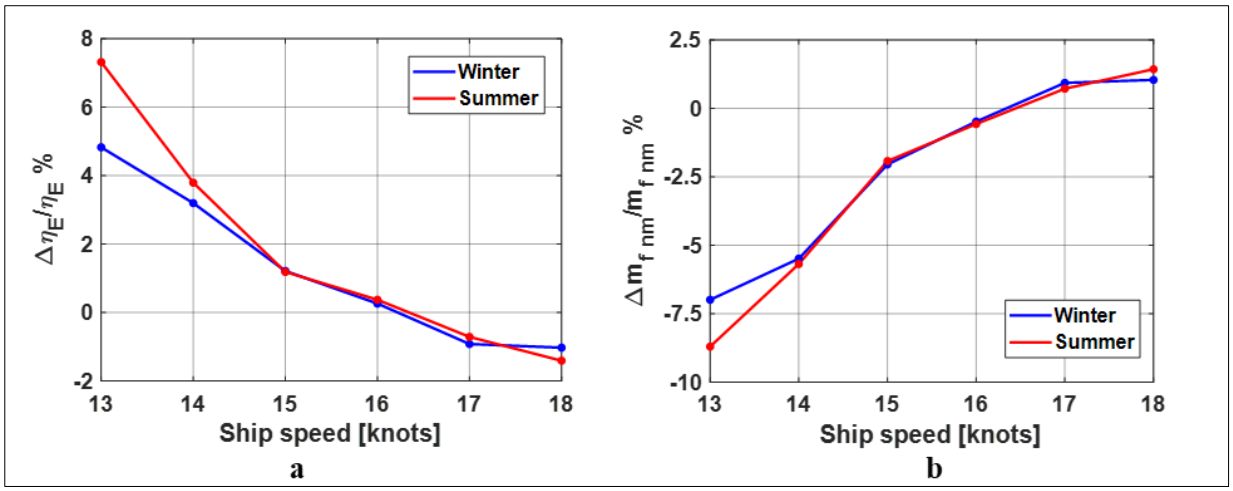

Figure 9 Percentage differences between the two Bergen engines, regarding engine efficiency (a) and fuel consumption per nautical mile (b), for different ship's speeds in winter and summer conditions

6. Conclusions

Using a computer code previously developed by the authors for the simulation of a traditional mechanical propulsion plant (composed by two independent axis lines) of an existing small cruise ship, the original diesel engines have been replaced (in the simulation) by a couple of two more modern design diesel engines, produced by the same manufacturer, with a nominal power almost the same, and similar to that of the original engine, but characterized by a specific fuel consumption contours trend, in the engine operating diagram, very different from each other. The article compares the two new engines by analyzing their main performance parameters, for different ship's speeds, in both winter and summer navigation conditions.

The main considerations drawn from the above reported engines comparison are the following:

- The 900 rpm N_{max} engine, due to the trend of its power limit curve in the engine operating diagram, requires a propeller *P/D* ratio reduction starting from 16 knots, while the same parameter reduction is required by the 1000 rpm N_{max} engine starting from 14 knots, due to the more favorable trend of its power limit curve in the engine operating diagram. This entails, by using the 1000 rpm N_{max} engine, a greater propeller efficiency and consequently a lower power demand by the propulsion engines when the ship speed decreases. This advantage increases in the winter navigation.
- At higher ship speeds (17-18 knots) the 900 rpm N_{max} engine has a slightly higher efficiency compared to the 1000 rpm N_{max} one. This advantage is cancelled at a speed of about 16 knots, and below this speed the 1000 rpm N_{max} engine works with a better efficiency than the 900 rpm N_{max} one. This advantage increases as the ship speed decreases, particularly during summer navigation.
- Due to the differences in the power required by the engines and to their efficiencies at different ship speeds and navigation seasons, the fuel consumption per nautical mile is very similar for the two engines at ship speeds equal or greater than 16 knots. At ship speeds below this value the fuel consumption gap becomes more and more marked in favour of the 1000 rpm N_{max} engine.

The comparison between the two engines, in the context of a marine propulsion plant characterized by propellers mechanically connected to the engines, shows a substantial equivalence between them around the ship's speed of 16 knots, with a slight advantage of the 900 rpm N_{max} engine at higher speeds (17-18 knots), and an advantage of the 1000 rpm N_{max} engine, always greater when the ship speed decreases from about 16 knots. The advantage of the 1000 rpm N_{max} engine becomes more consistent at lower ship speeds, especially in summer navigation.

The comparison carried out between the two engines, very similar but characterized, the first (900 rpm N_{max}) by a 'typical' trend of the specific fuel consumption in the engine operating diagram, the second (1000 rpm N_{max}) by an unconventional trend, led to the conclusion that in a 'mechanical' marine propulsion system, such as the one considered, the 1000 rpm N_{max} engine is, from an overall point of view, better than the 900 rpm N_{max} engine, mainly at low ship speeds.

These considerations were obtained from the comparison between two marine engines fuelled with traditional liquid fuels, but they are also valid in the case of engines fed with alternative fuels currently in use, such as natural gas, or likely to be used in the near future, such as: hydrogen, methanol and ammonia.

Compliance with ethical standards

Acknowledgments

The authors wish to acknowledge the support to the present research given by Rolls-Royce Marine technical office (United Kingdom) and by engineer Irene Zanin and mister Andrea Cerutti of Italian Rolls-Royce.

Disclosure of conflict of interest

The authors declare no conflict of interest.

References

[1] International Maritime Organization (IMO). Consideration of the energy efficiency design index for new ships - Proposals on the effect of generators and diesel-electric propulsion systems. GHG-WG 2/2. February 4, 2009.

[2] International Maritime Organization (IMO). Interim guidelines on the method of calculation of the energy efficiency design index (EEDI) for New Ships. MEPC.1/Circ.681. August 17, 2009.

[3] International Maritime Organization (IMO). Consideration of the energy efficiency design index for new ships - Recalculation of energy efficiency design index baselines for cargo ships. GHGWG 2/2/7. 4 February 4, 2009.

[4] International Maritime Organization (IMO). M2 Ship Energy Efficiency Regulations and Related Guidelines. London, UK. January 2016.

[5] Benvenuto G, Campora U, Carrera G, Casoli P. A Two-Zone Diesel Engine Model for the Simulation of Marine Propulsion Plant Transients. MARIND 98, Second International Conference on Marine Industry, Varna, Bulgaria, September 28 – October 2, 1998. ISBN: 9789547150539.

[6] Campora U, Figari M. Numerical Simulation of Ship Propulsion Transients and Full Scale Validation. Proc. Instn Mech Engrs. Vol 217 Part M: Journal of Engineering for the Maritime Environment, 2003, ISSN: 1475-0902.

[7] Altosole M, Benvenuto G, Campora U. Numerical Modelling of the Engines Governors of a CODLAG Propulsion Plant. 20th BLACK-SEA International Congress, Varna, Bulgaria, October 7-9, 2010, ISSN: 1314-0957.

[8] Altosole M, Balsamo F, Benvenuto G, Campora U. Numerical Modelling and Analysis of the Ambient Conditions Influence on the Performance of a Marine Diesel Engine. Development in Maritime Technology and Engineering – Guedes Soares & T. A. Santos (eds), CRC Press, Taylor & Francis Group, Balkema book, London, UK, Proceedings and Monograph in Engineering, Water and Earth Sciences, 2021, Copyright by the Authors, p. 463-12, ISBN: 978-0-367-77377-9, DOI: 10.1201/9781003216599-49.

[9] Rolls-Royce. Diesel and gas engines generator set and propulsion systems (Internal report), Rolls-Royce Marine. Bristol, UK. 2015.

[10] Durković R, Damjanović M. Regression Models of Specific Fuel Consumption Curves and Characteristics of Economic Operation of Internal Combustion Engines. Mechanical Engineering, Vol. 4, No 1, 2006, p. 17-10, UDC 621.437:629.4.082.2.

[11] Eleftherios KD, Dominic AH, Stephen RT. Assessing the Potential of Hybrid Energy Technology to Reduce Exhaust Emissions from Global Shipping. Energy Policy 40, 2012, p. 204-15, DOI: 10.1016/j.enpol.2011.09.046.

[12] MAN 51/60 DF IMO TIER II / IMO TIER III, Project Guide – Marine, 2015.

[13] Yazaki A. Further Model Tests of Four Bladed Controllable Pitch Propellers. Ship Research Institute, Paper 16, Tokyo, Japan, 1966.

[14] Farzaneh-Gord M. The First and Second Law Analysis of a Spark Ignited Engine Fuelled with Alternative Fuels. Archives of thermodynamics 30, p. 73-20, 2009.

[15] Zahdeh AR, Henein NA, Bryzik W. Diesel Engine Cold Starting: P-C Based Comprenhensive Heat Release Model: Part I - Single Cycle Analysis. ASME Transaction, Journal of Engineering for Gas Turbines and Power, Vol. 113, July, p. 464-12, 1991.

[16] Sorenson SC. Simpler Computer Simulations for Internal Combustion Engine Instruction. International Journal of Mechanical Engineering Education, Vol. 9, n° 3, 1981.

[17] Heywood JB. Internal Combustion Engine Fundamentals. McGraw-Hill, New York, USA, 1988